

Millimeter-wave photonic wireless links for very high data rate communication

Jin-Wei Shi¹, Chen-Bin Huang² and Ci-Ling Pan^{2,3*}

National Central University and National Tsing-Hua University, Taiwan

In this paper, recent progress in millimeter-wave (MMW) photonic gigabit wireless communication is reviewed. This technique is attractive partly because the MMW signal can be easily distributed from central to base stations through the use of a low-loss optical fiber. This radio-over-fiber approach facilitates the transmission of MMW signals. An MMW photonic transmitter, comprised of high-power photodiodes with integrated antennas for MMW signal broadcasting, is needed for signal generation only over the last mile. The development of several different low-noise optical MMW sources and high-power photonic transmitters and photodiodes for optical MMW wireless links is summarized. The performance of photonic wireless links with extremely high data rates ($>10\text{ Gbit s}^{-1}$) developed based on these key components and using different modulation schemes is also reviewed. Finally, some advanced commercially available products and the prospects of a future gigabit wireless communication era are discussed.

The most useful wireless communication band is located in the frequency range of 0.3–3.5 GHz for reasons of compact antenna size, low propagation loss and good penetration through buildings [1]. However, wireless carrier frequencies are being pushed higher due to emerging high-bandwidth applications, which include next-generation smart cell phones [1] and wireless linking for three-dimensional super high-definition television [2]. As a result, the millimeter-wave (MMW) bands at 60 (V-band), 120 (D-band) and even higher than 300 GHz are beginning to attract attention due to their ‘unlicensed’ usage [2–8].

Several key front-end components have been developed employing the already mature silicon-based complementary metal–oxide–semiconductor (CMOS) integrated-circuit (IC) technology for wireless communication in the V (50–75 GHz) and W (75–110 GHz) bands or even higher operating frequencies for wireless communication [9]. Recently, a 60 GHz CMOS transceiver module [10] and system comprised of antennas, 60 GHz power amplifiers, local oscillators and baseband ICs has been commercially developed by SiBEAM (USA). In addition, advanced InP-based high electron mobility transistors (InP-HEMTs) and heterojunction bipolar transistors have been used to develop some high-speed ICs and key components that operate at 125 GHz [11,12] or greater than 300 GHz [13,14] for $>1\text{ Gbit s}^{-1}$ wireless communication systems.

However, MMW signals suffer substantial propagation loss in free space [8]. This problem and their inherent straight-line path of propagation affect connections and synchronization between the different parts of the whole communication system [15]. A promising solution to overcome this problem is the radio-over-fiber (RoF) technique [3,4,16,17], in which the MMW local-oscillator signal and data are both distributed through a low-loss optical fiber and only radiated over the last mile to the end user. Figure 1 shows a schematic representation of this approach, illustrating the motivation and working principles of two MMW-over-fiber communication systems. Figure 1(a) shows the additional electrical-to-optical (E–O) and optical-to-electrical (O–E) conversion processes used in the central office and base station,

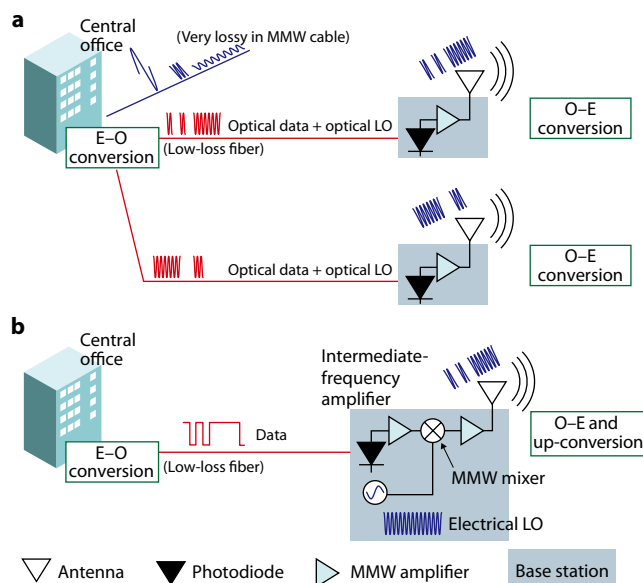


Figure 1. Conceptual diagrams of MMW-over-fiber communication systems with (a) a common optical local oscillator (LO) MMW source shared by different base stations and (b) different electrical LO MMW sources installed at each base station.

respectively. The optical MMW signal is distributed remotely through a low-loss fiber from the central office to several base stations, effectively eliminating the huge propagation loss of the MMW signal that occurs in an electrical transmission line or free space. Figure 1(b) shows another possible solution for the realization of a photonic wireless link, where only the optical data signal is distributed from the central office to each base station through optical fiber links. At the base station, a wideband photodiode, an oscillator, a mixer, an amplifier and an antenna operating in the MMW bands are used to up-convert, mix and amplify the

*Corresponding author. Email: clpan@phys.nthu.edu.tw

¹Department of Electrical Engineering, National Central University, Taoyuan 320, Taiwan

²Institute of Photonics Technologies, National Tsing-Hua University, Hsinchu 300, Taiwan

³Department of Physics, National Tsing-Hua University, Hsinchu 30013, Taiwan

incoming optical data to electrical MMW signals for radiation to the end user over the last mile. The base stations in Figure 1(b) are more expensive and complex compared with those in the architecture shown in Figure 1(a), where each base station is synchronized and shares the same optical MMW local-oscillator signal. This is because high-cost MMW ICs, which include the above-mentioned elements (mixer, oscillator and amplifier for the MMW bands), are necessary at each station. In addition, it remains a challenge to synchronize the different MMW oscillators at different base stations, which may be an issue for mobile users roaming among different base stations [15]. We can thus conclude that in order to realize a high-performance photonic-wireless link, a high-quality optical MMW source in the central office and a high-power photodiode-integrated MMW antenna (*i.e.* photonic transmitter) at the base station are essential.

Recently, a number of research groups at NTT reported excellent results for a 10 Gbit s⁻¹ line-of-sight wireless linking at 120 GHz, which was achieved using a uni-traveling carrier (UTC) photodiode-based photonic transmitter [3] with an on-off keying (OOK) data format and direct modulation on the 120 GHz optical carrier wave. By further increasing the optical local oscillator frequency (>300 GHz), a higher data rate (>10 Gbit s⁻¹) can be expected [6]. In addition, using the advanced modulation formats in the RoF system, such as the 16-quadrature amplitude modulation (16-QAM) and orthogonal frequency-division multiplexing (OFDM) techniques, research teams in Germany and Taiwan have achieved data rates of up to around 30 Gbit s⁻¹ at 60 GHz [18,19]. Two key components play important roles in these high-performance RoF communication systems with such high carrier frequency (*i.e.* MMW) and data rate. One is the photonic MMW source [20–23], which should deliver a stable, clean and less-dispersive optical signal with a high-modulation-depth MMW envelope for remote generation of electrical MMW signals at the base station. The other is the photonic transmitter [24–27], which is composed of a high-speed, high-power photodiode and high-directivity antenna. During operation, such a device can convert the intense optical signal to a strong electrical MMW signal that can be efficiently radiated to the end user. Compared with using the MMW electrical amplifier to further amplify a weak electrical signal from the high-speed photodiode, a combination of an erbium-doped fiber amplifier and high-power, high-speed photodiode can convert the intense optical signal to a strong MMW signal directly. This not only releases the burden imposed on the MMW amplifier but also provides superior noise performance [28,29]. With the integration of a high-directivity antenna, it should be possible to achieve high gain (directivity) in the broad frequency regime and radiate the wideband digital data carried on the MMW wave efficiently [30–32].

In the following section, we review recent progress related to different kinds of photonic MMW sources and high-power, high-speed photodiodes with different material systems that operate up to the sub-THz frequency regime. The improvement in the data rate of modern MMW RoF systems will then be addressed. Finally, we will discuss the challenges and prospects of future work on the MMW RoF system.

Optical millimeter-wave sources

In this section, the development of several high-performance optical MMW sources with modulated central frequencies from 60 GHz up to hundreds of GHz is reviewed, and the advantages and disadvantages of different approaches are discussed. Although subharmonic mode-locked laser diodes have been reported for MMW signal generation up to 240 GHz [33,34], the mode-locking electrical signal (at 80 GHz) required for operation at this frequency is itself not easily accessible. This leads to the simplest approach being used to realize a photonic MMW source with a wide frequency tuning range (from near 0 Hz to several THz): the two-laser heterodyne beating system [35,36]. In this approach, by sweeping the wavelength difference between two tunable continuous-wave (CW) lasers, a photonic MMW carrier can be flexibly obtained through coherent interference. Taking a central wavelength of

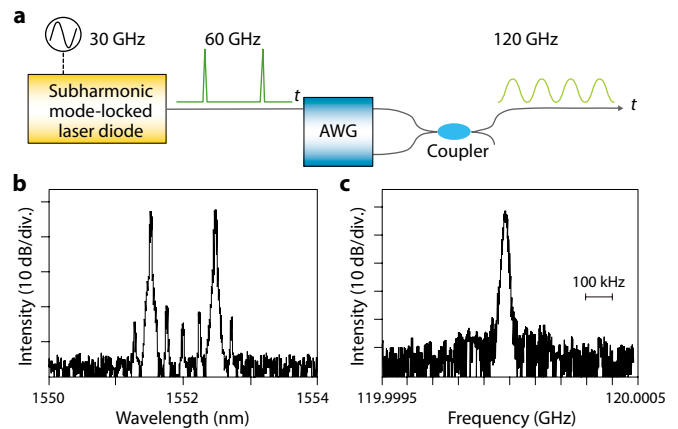


Figure 2. (a) Schematic representation of a subharmonic mode-locked semiconductor laser with AWG filter setup for photonic 120 GHz MMW signal generation. (b) Measured optical spectrum with 120 GHz line spacing, and (c) measured MMW spectrum at 120 GHz (adapted from Ref. 41 © 2003 IEEE).

1,550 nm as an example, a 0.8 nm wavelength difference corresponds to a 100 GHz MMW frequency. Using this method, wireless data transmission has been demonstrated in the 300 GHz to 1 THz MMW carrier frequency regime [2,6]. Although highly agile, the nature of interference with this method demands highly synchronized lasers, otherwise large phase noise will accumulate in the resulting photonically generated MMW signal. One solution for obtaining MMW and THz signals with low phase noise is to synchronize two lasers of narrow linewidth (hundreds of kHz), as has been demonstrated for the 830 nm range [37]. However, such a system is complex and stability remains an issue for practical application in communication systems.

A homodyne beating system, in which the photonic MMW signal results from the interference between two or more optical frequency components derived from a single laser, is a good alternative as a photonic MMW source [38]. Instead of using a mode-locked laser that requires complicated stabilization schemes and often results in low-frequency spacing, a stable frequency comb source can be obtained by externally modulating a CW laser. A common approach is to inject a narrow-linewidth CW laser into an electro-optical phase/intensity modulator, which is then applied with a strong radiofrequency sinusoidal modulation signal for side-band generation [39,40]. The resulting frequency comb spacing is equal to the modulation (radio)frequency. Photonic MMW signals with frequencies of integer multiples of the comb spacing can be generated after applying an optical amplitude or phase filter to the frequency comb.

Recently, several research groups [2,3,20,41] have demonstrated high-quality photonic MMW signal generation at 120 GHz to around 300 GHz [20,41] utilizing this technique with an arrayed waveguide grating (AWG) as the amplitude optical filter. A conceptual diagram of such a system is shown in Figure 2 [41]. The AWG effectively filters every other comb line, resulting in an optical spectrum with comb line spacing of 120 GHz and a measured MMW spectrum with central frequency of 120 GHz. As can be seen from the figure, the resulting photonic MMW signal has high modulation depth because the two comb lines are of almost equal height. The MMW signal is also relatively noisy as indicated by the moderate side-mode suppression ratio (SMSR; >25 dB). Despite these excellent results, however, there remain challenges with such a technique. In order to obtain a low-noise MMW optical envelope with a 100% modulation depth, the magnitude of these two comb lines must be exactly equal. As the output comb spectral profile coming directly from the modulator typically shows amplitude variations, a high-performance AWG filter with a high extinction ratio and a specially designed transfer function [42] is needed in order to compensate for the unevenness. Planar lightwave circuits are also temperature sensitive. Therefore, either active thermal control is required

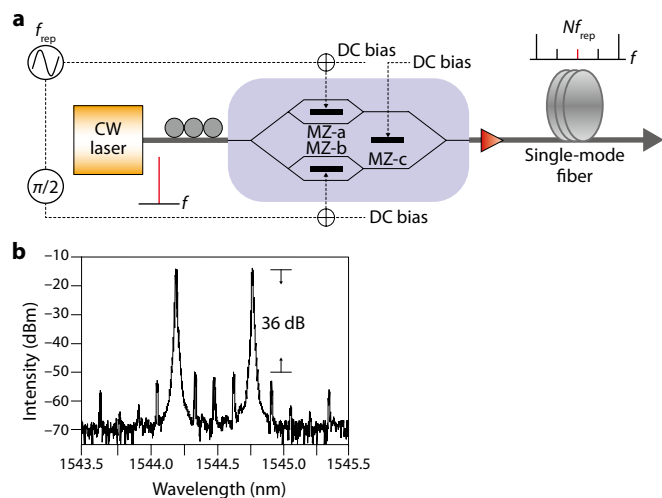


Figure 3. (a) Schematic representation of a dual parallel MZM setup for photonic MMW signal generation. (b) Measured optical spectrum with 72 GHz line spacing (adapted from Ref. 44 © 2008 IEEE).

or athermal packaging becomes critical. Another side issue with the use of amplitude filtering is that the majority of the CW laser injected power is lost.

Recently, through careful application of bias and modulation controls to a dual-parallel electro-optical Mach-Zehnder modulator (MZM), a ‘filterless’ optical MMW source for frequencies up to 300 GHz (after frequency 12-tupling) has been successfully demonstrated [43,44]. Figures 3(a) and (b) show a conceptual diagram of this system and the measured optical spectrum [44]. The dual-parallel MZM serves as a key component for the 10 GHz spacing phase tuned optical frequency comb. This approach not only eliminates the huge optical loss during amplitude filtering, but also offers a higher SMSR (>30 dB) for the resulting photonic MMW signal [43,44], as shown in Figure 3(b). As no optical filter is required, the proposed system can also be utilized in wavelength division multiplexing up-converted systems [44].

Another powerful solution is to further process the externally modulated CW laser frequency combs using spectral line-by-line pulse shaping [45]. Compared with passive AWG, the line-by-line shaper is an adaptive setup and can therefore offer complete gray-level control in terms of optical phase, amplitude and even polarization. Figures 4(a) to (c) show a typical setup incorporating a line-by-line pulse shaper for photonic MMW generation, the optical spectrum of the 100 GHz two-line sinusoidal signal and the optical spectrum of the 100 GHz short-pulse (~2 ps) signal with four comb lines, respectively [22]. The details of a typical reflective line-by-line shaper are included in Figure 4(a). Such a line-by-line pulse shaper consists of a fiber-pigtailed collimator with 3.5 mm spot diameter, which is used to send the comb to a 1,200 groove/mm gold-coated grating. Discrete comb lines are diffracted by the grating and focused by a lens with a focal length of 400 mm. A fiberized polarization controller is used to adjust for horizontal polarization on the grating. A computer-controllable 2×640 pixel liquid-crystal modulator array is placed immediately before the focal plane of the lens to independently control the amplitude and phase of individual spectral lines. A retro-reflecting mirror placed on the Fourier plane of the lens gives a double-pass geometry, where all spectral lines recombine into a single fiber and are separated from the input via an optical circulator. Combined with a polarizer placed between the collimator and the grating, control of gray level intensity can be achieved with a maximum extinction ratio of up to ~27 dB, limited by the liquid-crystal modulator. The fiber-to-fiber insertion loss of the pulse shaper is below 6 dB. Several applications of such a system have been reported, for example, for rapid-reprogrammable arbitrary microwave waveform generation [46] as well as for the tailoring of microwave power spectra [47].

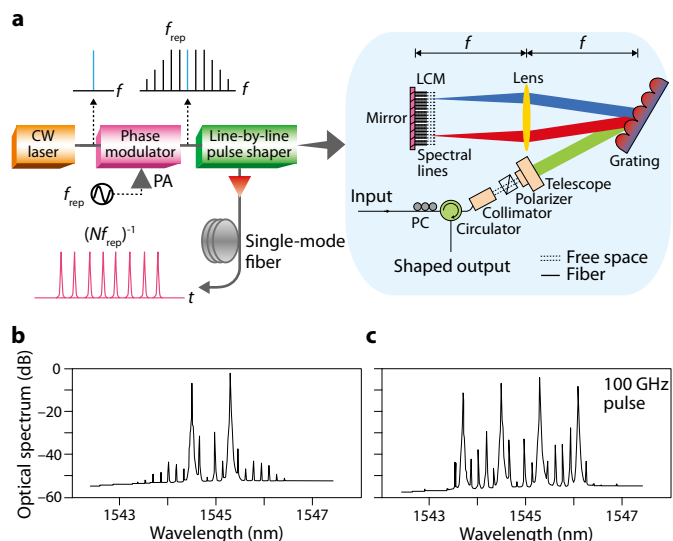


Figure 4. (a) Schematic representation of a line-by-line pulse shaper setup. (b,c) Measured optical spectra of 100 GHz two-line (b) and 100 GHz four-line (c) combs (adapted from Ref. 22 © 2010 IEEE).

Utilizing this setup, ~1 ps optical pulse trains with 31–496 GHz repetition rates suitable for remote high-modulation-depth photonic MMW generation have been demonstrated [48]. Compared with the use of pure optical sinusoidal waveforms as the photonic MMW source, short optical pulse excitation could offer a ~7 dB enhancement in the resulting MMW power given the same average operation photocurrent. In addition, a higher maximum saturation current is obtained due to reduced device heating [22]. Furthermore, the line-by-line shaper can simultaneously provide the dispersion pre-compensation required for delivering short optical pulses for remote (>25 km) MMW signal generation without the need for additional dispersion management within the fiber link [48].

Efforts in laser engineering have also accomplished various interesting photonic MMW signal generation results. By creating dual-wavelength laser outputs, the photonic generated MMW signal frequency is defined by the frequency difference between the two modes. In one typical approach, tunable dual-wavelength separation can be accomplished by controlling the optical filters to be used either for laser self-injection [49–51] or external filtering [52]. Another method utilizes nonlinear semiconductor laser dynamics, where the output of a master laser diode is injected into a slave laser diode [53–55]. As injection is unidirectional, the slave laser does not alter the behavior of the master laser. Careful selection of the injection operational parameters (bias current of the slave laser, injection power of the master laser into the slave and frequency detuning between the master and the slave lasers) can then initiate the nonlinear dynamical state of the slave laser [53]. Recently, this approach has been utilized to demonstrate MMW signal generation at 120 GHz [55].

Millimeter-wave photonic transmitters

In this section, we review the development of several kinds of sub-THz photonic transmitters and photomixers for the MMW or THz frequency regime. The photonic transmitters for such applications are constructed by integrating high-power photodiodes with antennas for converting an intense optical MMW signal to an electrical signal, and then radiating that signal to the end user. Compared with the approach of using several MMW amplifiers to further amplify the small photocurrent from a high-speed photodiode, the combination of high-speed, high-power photodiodes with a high-power erbium-doped fiber amplifier is an attractive alternative to costly, narrow bandwidth, noisy electrical MMW amplifiers with limited gain and saturation power

performance [29]. The (peak) saturation-current-bandwidth product (SCBP) is a key parameter for evaluating the performance of these high-power, high-speed photodiodes [28,29,56–59]. By increasing the saturation current of the photodiode, it is possible to boost the injected optical power and further increase the maximum available MMW power produced therefrom. The saturation current density of a photodiode can be obtained by the following equation:

$$J_{\max} \approx (V_{\text{bias}} + \Phi) \frac{\varepsilon V_{\text{carrier}}}{D^2} \quad (1)$$

where J_{\max} is the maximum output current density from the photodiode, V_{bias} is the reverse bias voltage, Φ is the built-in potential of the photodiode, ε is the dielectric constant in the depletion region, V_{carrier} is the effective drift velocity of the photogenerated carriers (including the drift velocity of electrons and holes [28]) and D is the depletion layer thickness. As can be seen, a thinner depletion layer, higher effective carrier drift velocity, or higher reverse bias voltage should improve the maximum output current density of the photodiode. The maximum V_{bias} of the photodiode is limited by the thermal failure of the device and the breakdown field of the depletion layer, which can be improved by appropriate device packaging with careful consideration of heat-sinking [58] and by increasing the depletion layer thickness, respectively. However, the latter approach conflicts with equation (1) above, which states that J_{\max} can be greatly increased by downscaling D . In most practical high-power photodiodes, the maximum output current from the photodiode and its allowable bias voltage are more heavily dependent on the thermal package than the breakdown field in the depletion layer. Downscaling the thickness of the depletion layer thus becomes the most effective way to shorten the carrier transit time and attain high saturation current performance [58,59]. However, a thin depletion layer thickness is always accompanied by a large junction capacitance, which causes a significant trade-off between the saturation current and the resistance–capacitance-limited bandwidth of the photodiode. The key means of achieving the ultimate high SCBP for photodiodes is therefore to downscale the photo-active absorption area as well as the thickness of the depletion layer [58,59].

Low-temperature-grown (LTG) GaAs materials and devices have been developed specifically for easing this trade-off between resistance–capacitance-limited bandwidth and carrier drift time. LTG-GaAs is prepared through molecular beam epitaxial growth at 200 °C instead of the usual 600 °C. After growth, however, proper *in situ* or *ex situ* annealing at 600 °C is necessary in order to increase the density of arsenic precipitates and hence resistivity of this layer [60]. A high density ($>10^{18} \text{ cm}^{-3}$) of arsenic precipitates in LTG-GaAs results in excess arsenic-related point defects and a short carrier trapping time [61]. Due to the high resistivity and extremely short carrier trapping time (~ 200 fs) of LTG-GaAs, carrier drift time, dark current and depletion layer thickness are of considerably less importance for the construction of high-power, high-speed LTG-GaAs-based photodiodes. LTG-GaAs-based metal–semiconductor–metal photodiodes [62–64], photoconductive dipole antennas (PDAs) [8,65,66], and p–i–n photodiodes [59,67] with extremely high saturation peak output power and wide O–E bandwidth have been demonstrated. High-power LTG-GaAs-based photodiodes have been used with planar-circuit broadside antennas, including planar dipole, slot and spiral antennas [68].

Several sub-THz and THz LTG-GaAs-based photomixers and PDAs have been successfully demonstrated. A silicon lens is usually integrated onto the substrate of the photomixer in order to minimize the substrate mode problem and enhance the radiating power (efficiency) of these integrated broadside antennas, which are designed to operate in the near-THz frequency regime [24,68]. Significantly higher CW and pulse THz output power has been reported for LTG-GaAs-based photomixers compared with that achieved by traditional p–i–n photodiodes [59,67]. Figure 5(a) shows an LTG-GaAs-based photomixer module with an integrated spiral antenna and a silicon-substrate lens for THz frequencies [68], and Figure 5(b) shows the measured frequency response of

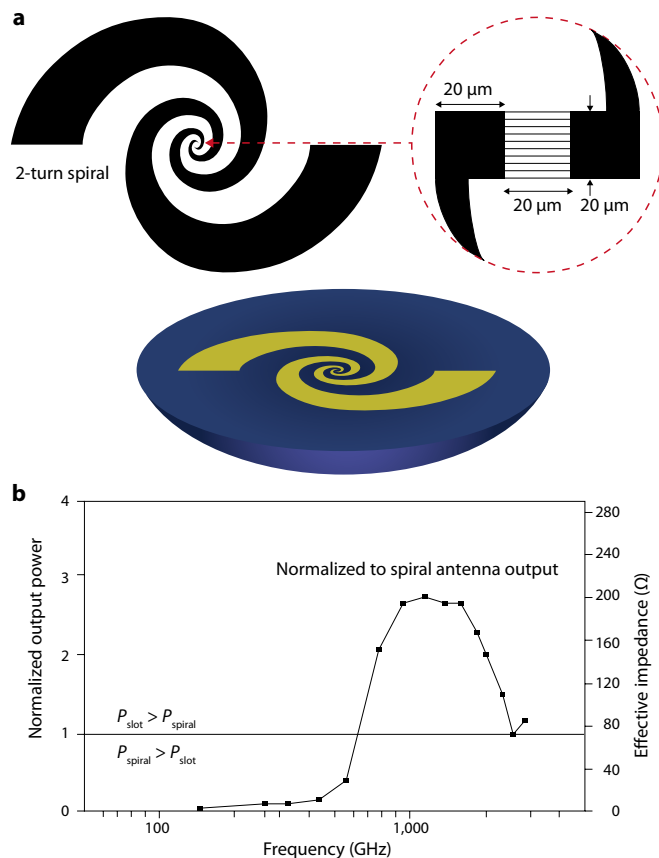


Figure 5. (a) Top view of an LTG-GaAs-based photomixer integrated with a spiral antenna and silicon lens for THz radiation. (b) Measured frequency response of an LTG-GaAs-based photomixer with integrated slot antenna (normalized to the output power of the spiral antenna) (adapted from Ref. 68 © 1997 IEEE).

such an LTG-GaAs photomixer integrated with another slot antenna. As can be seen from the figure, the slot antenna provides much higher output power in the 1–2 THz frequency regime compared with the spiral antenna due to the characteristic resonance of the slot antenna [68]. These LTG-GaAs-based PDAs have been successfully used for wireless linking at center frequencies of around 0.3 THz [65,66]. However, the data rate so far achieved is low ($\sim 1 \text{ Mbit s}^{-1}$) [65] and limited by the repetition rate of the Ti:sapphire laser ($\sim 80 \text{ MHz}$). In addition, the internal quantum efficiency of these LTG-GaAs-based devices is poor, usually less than 10%, due to the short carrier trapping time. Aside from these issues, the most serious problem limiting the potential of LTG-GaAs-based devices for high-data-rate communication is the different carrier trapping and recombination time constants [69]. Compared with the short trapping time (~ 200 fs), the photogenerated carriers inside the active LTG-GaAs layer are subject to much longer recombination times in the defect states (~ 1 ns vs ~ 200 fs) [69]. Under high-power CW operation, these non-recombined carriers may accumulate in the defect states, which can seriously degrade the power and speed performance of LTG-GaAs-based photonic transmitters. In addition to increasing the bias voltage and downscaling the depletion layer thickness as discussed above, the most attractive way to further improve the saturation current without sacrificing the speed performance of the photodiode is to increase the carrier drift velocity (see equation (1)).

Many III-V-based semiconductor materials, such as $\text{In}_{0.55}\text{Ga}_{0.45}\text{As}$, InAs and InSb, have been reported to have extremely high electron mobility in the infrared wavelength regime. However, during photodiode operation, photogenerated holes with slow drift velocity are always a major factor limiting speed. The ‘slow’ hole problem is eliminated in the InP-based UTC photodiode structure [28,70,71] and in near-ballistic

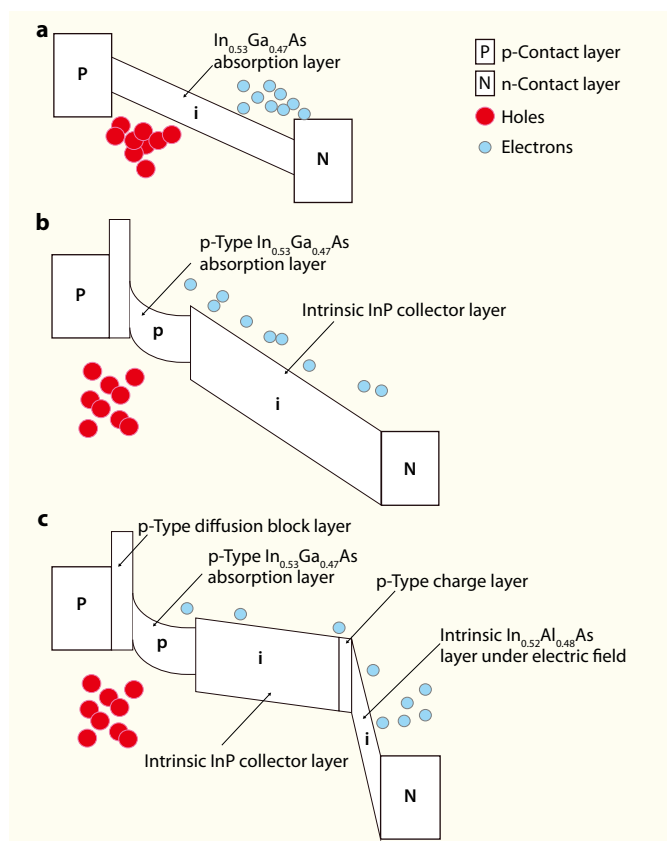


Figure 6. Conceptual band diagrams for (a) p-i-n, (b) UTC and (c) NBUTC photodiodes

UTC (NBUTC) photodiodes [56–58,72–74], where only electrons with high drift velocity act as active carriers. Figure 6 shows conceptual band diagrams for p-i-n, UTC and NBUTC photodiodes. Under optical power illumination, the photogenerated holes in the p-i-n photodiode (Figure 6(a)) accumulate in the active absorption layer due to their much lower mobility compared with electrons. This phenomenon will induce a significant space-charge field that screens the external applied electric field, resulting in serious speed degradation. In such a case, it is necessary to increase the reverse bias voltage to further increase the saturation current up to the thermal failure limit. The problem of hole transport is eliminated in the UTC photodiode (Figure 6(b)) because the photo-absorption process only occurs in the p-type $\text{In}_{0.53}\text{Ga}_{0.47}\text{As}$ layer instead of in the intrinsic absorption layer as in the traditional p-i-n photodiode. In the p-type absorption layer, photogenerated holes are the majority carrier and should relax directly to the anode of the UTC photodiode without transport [28]. Photogenerated electrons, on the other hand, will diffuse through the p-type absorption layer and drift to the InP depletion and cathode layers. The bandgap of the InP layer is large enough to avoid the photo-absorption process under excitation at a wavelength of 1.55 μm . It can thus be understood that electrons are the only active carriers in the UTC photodiode structure. This leads to a significant improvement in the effective carrier drift velocity of the photodiode during operation and excellent SCBP performance [28,70,71].

The major difference between the UTC photodiode and the NBUTC photodiode is the insertion of an additional p-type charge layer in the collector layer to control the distribution of the internal electrical field, which results in an over-shoot of the electron drift velocity even under high reverse bias voltage (-3V) [56–58,71–74]. Figure 6(c) shows a conceptual band diagram for an NBUTC photodiode. A thin p-type $\text{In}_{0.52}\text{Al}_{0.48}\text{As}$ charge layer in the InP-based collector layer experiences most of the externally applied electric field due to the higher breakdown field compared with that of InP. Based on equation (1), the higher electron drift velocity in the NBUTC photodiode suggests that

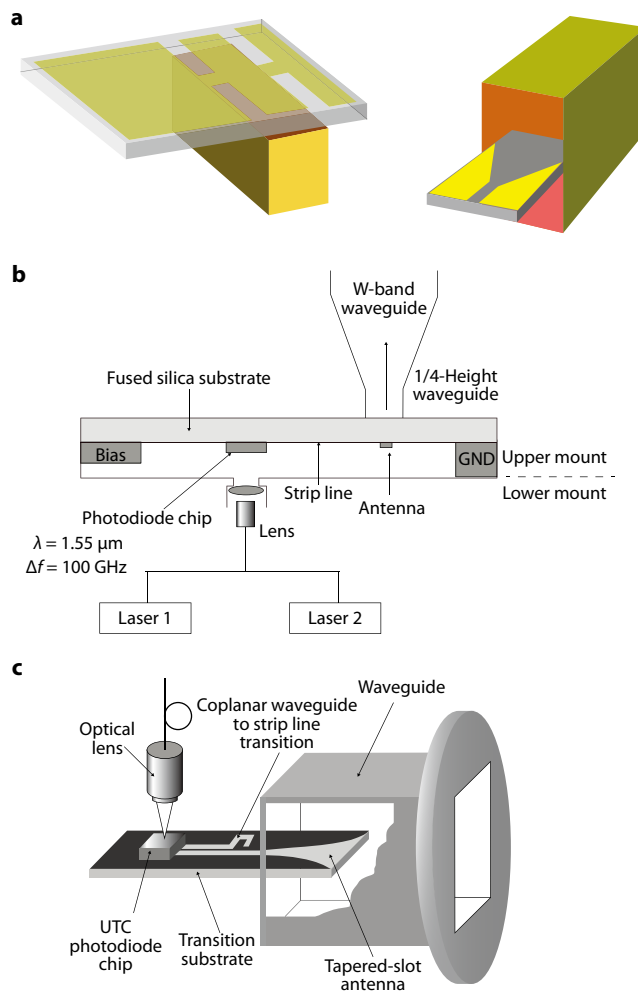


Figure 7. (a) Conceptual schematic diagrams of a broadside patch antenna (top) and an end-fire tapered slot antenna (bottom) for rectangular waveguide excitation (adapted from Ref. 30 © 2004 IEEE). (b,c) Conceptual cross-sectional diagram of a UTC photodiode-based photomixer with integrated patch antenna (b) and tapered slot antenna (c) for WR-10 and WR-08 waveguide excitation, respectively (adapted from Ref. 76 © 2004 IEEE).

these devices could offer superior SCBP performance compared with UTC photodiodes. The reported SCBP for a single UTC photodiode is usually around the 2,500 mA GHz level [28,70,71]. With this NBUTC device we have demonstrated an SCBP of over 4,070 mA GHz [58], and a NBUTC photodiode with a linear cascade structure has been reported to have an SCBP of as high as 7,500 mA GHz, the highest achieved so far [56,57]. The excellent performance of UTC and the NBUTC photodiodes in terms of speed and saturation power means that high-performance photonic transmitters with an end-fire or broadside radiation pattern [24,25,30,75,76] and operating frequency of 0.1–1 THz can be realized, along with a much higher output power ($>20\text{ dB}$) compared with p-i-n [77] and LTG-GaAs-based photonic transmitters [70].

Figure 7 shows a UTC photodiode-based photonic transmitter with a broadside (patch) antenna [76] and end-fire (tapered slot) antenna [30] for the excitation of WR-10 and WR-8 rectangular waveguide-based horn antennas. Using these modules, 10 Gbit s^{-1} wireless line-of-sight data transmission at a center frequency of 120 GHz has been demonstrated [3]. Recently, our group has also demonstrated the use of an NBUTC photodiode-based photonic transmitter with a quasi-Yagi radiator for excitation of a WR-10 waveguide-based horn antenna [75,78–80]. Figure 8 shows a conceptual diagram of a quasi-Yagi radiator for rectangular waveguide excitation, a top view of the NBUTC photodiode-based photonic transmitter and a photograph

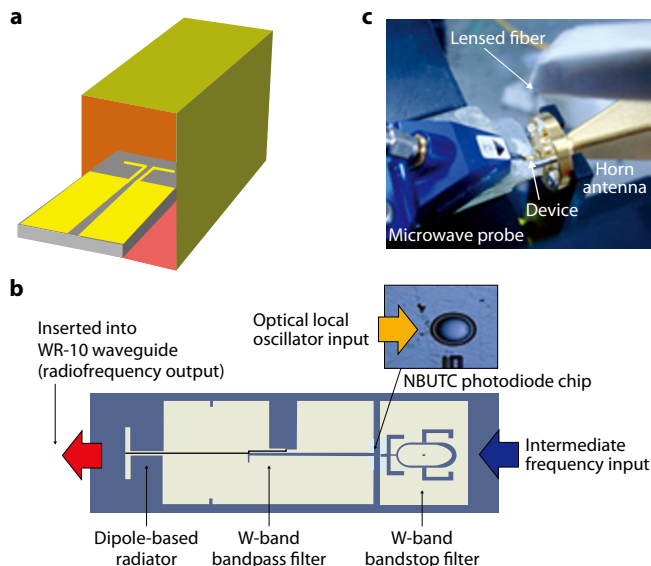


Figure 8. (a) Conceptual schematic diagram of an end-fire quasi-Yagi antenna for rectangular waveguide excitation. (b) Top view of a NBUTC photodiode-based photonic transmitter integrated with quasi-Yagi antenna for WR-10 waveguide excitation. (c) Photograph of an actual device during measurement.

of an actual device. The quasi-Yagi radiator is comprised of a half-wavelength dipole element and a ground reflector, making the device significantly more compact than the traditional tapered slot antenna used for rectangular waveguide feeding (normally several wavelengths in length). Antennas of this sort are relatively immune to substrate modes [31,32,75]. Compared with the traditional UTC photodiode-based photonic transmitter, this device incorporates an additional intermediate frequency input port and two different W-band (bandpass and bandstop) filters for simultaneously realizing ultra-wide O–E and bias modulation (switching) bandwidth [79,80]. Under bias modulation, error-free wireless data transmission at 12.5 and 20 Gbit s⁻¹ has been successfully demonstrated [78–80]. In contrast to UTC photodiode-based photonic transmitters under bias modulation [81], the variation in the detected MMW power of this NBUTC photodiode device is due to its significant bias-dependent speed performance rather than due to variations in photocurrent [78]. For the case of UTC photodiodes, bias-dependent nonlinearity originates mostly from changes in photocurrent when the bias voltage is swung into forward bias, imposing a limit on modulation speed [81].

Photonic millimeter-wave wireless links

In this section, we review progress in the development of photonic MMW wireless links with very high data rates (>1 Gbit s⁻¹). Several windows are commonly used for MMW wireless data transmission, including the 60 GHz, W (75–110 GHz) and 120 GHz bands. The 60, 120 and >300 GHz bands are ‘license free’ because these frequencies correspond to the absorption peaks in free space [5,8]. These bands are thus suitable for indoor wireless data transmission, such as for connecting household appliances like high-definition televisions (HDTVs), cell phones and laptops, at high data rates (>1 Gbit s⁻¹). Recently, the 16-QAM or OFDM modulation formats have been used to achieve wireless data transmission of around 30 Gbit s⁻¹ at a 60 GHz center frequency [18,19]. The W-band has much lower propagation loss and a broader transmission window compared with the 60 and 120 GHz bands, and has been specified as the window for outdoor ‘gigabit’ wireless data transmission in several countries [5]. Recently, a number of research groups have demonstrated high-performance photonic-wireless linking in this band [78–80,82,83]. In our recent work, we demonstrated error-free 20 Gbit s⁻¹ OOK wireless data transmission in the W-band using

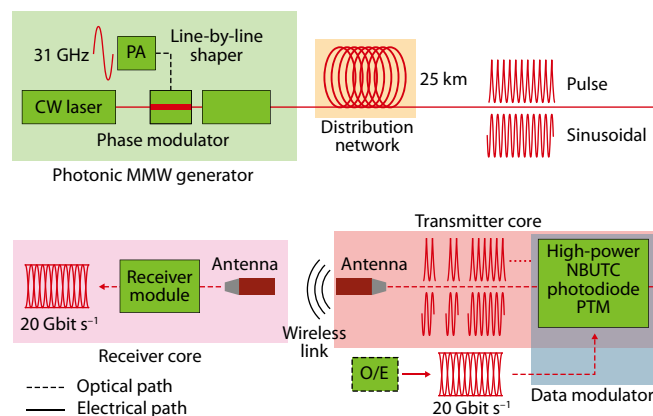


Figure 9. Conceptual diagram for a photonic wireless linking system for 20 Gbit s⁻¹ data transmission using a line-by-line pulse shaper as the photonic MMW source.

an NBUTC photodiode-based photonic transmitter–mixer [80]. The system setup is shown in Figure 9 [79,80]. This device includes a line-by-line pulse shaper, which serves as the MMW photonic source for sinusoidal or pulse signal generation at a center frequency of around 100 GHz. The data signal used for bias modulation in this photonic transmitter can be at another optical wavelength, which is converted to electrical 20 Gbit s⁻¹ data through the use of another low-speed photodiode. Using a bias modulation technique for remote signal up-conversion to the W-band at the base station, a long fiber transmission distance with less dispersion can be achieved [78–80].

Although larger available bandwidth for data transmission can be expected by further boosting the center frequency of the MMW to near 1 THz, the bandwidth and speed of the other active/passive MMW components and instruments for data transmission cannot follow simultaneously [6]. This truly limits the maximum allowable transmission data rate. In this high-frequency regime (>110 GHz), a fast MMW power detector, which has a wide video bandwidth, is usually adopted at the front-end of the receiver to down-convert the incoming MMW signal and acquire the data envelope. Using such a technique (envelope detection), 20 Gbit s⁻¹ error-free wireless data transmission at a center frequency of 93 GHz has been demonstrated [80]. Comparison is made with the reported 16-QAM, OFDM or differential phase-shift keying modulation formats [82,83]. The OOK modulation formats, despite providing extremely high data transmission rates (>12.5 Gbit s⁻¹) [6,80], incur serious problems with regard to the multi-path effect and occupy a larger bandwidth for the same desired data rate. However, a solution could be to develop a receiver with a much more compact and simpler architecture for OOK data detection [6,80]. Using the advanced InP–HEMT foundry, single-chip complex modulation and demodulation processes for 10 Gbit s⁻¹ quadrature phase-shift keying data have been demonstrated for 125 GHz wireless transmission [11]. Compared with the reported OOK 10 Gbit s⁻¹ data transmission [3], this solution offers the same data rate with only half the wireless bandwidth, reduced multi-path effect, and more compact receiver size. The progress in high-speed IC technology thus provides an effective way to optimize trade-offs between the total transmission data rate, the occupied wireless bandwidth, the multi-path effect and the size of transceiver module in a photonic wireless linking system.

Prospects

Practical applications of photonic MMW wireless linking can be found in the fields of HDTV broadcasting [84], as demonstrated by the NTT and NHK corporations in Japan. An uncompressed high-definition serial digital interface (HD-SDI) signal is desirable during live broadcasting, requiring a data rate of 1.5 Gbit s⁻¹ per channel. However, this is much faster than the rate achievable using state-of-the-art microwave

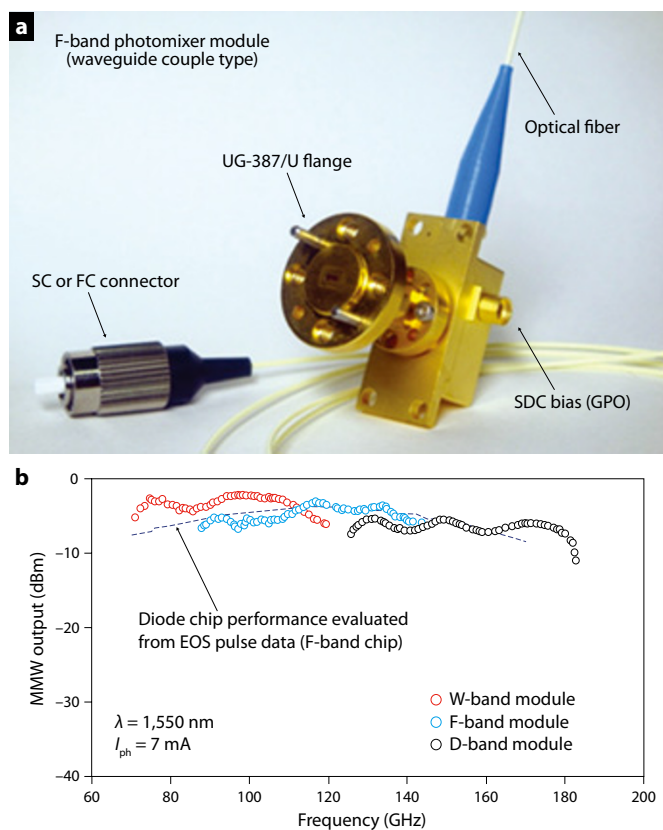


Figure 10. (a) Photograph of a commercial UTC photodiode-based photonic transmitter (© NTT). (b) Measured O–E response under fixed output photocurrent (7 mA).

field pick-up units. MPEG or JPEG2000 encoders are therefore adopted in current microwave wireless links to compress the HD-SDI signal, but this can cause time delays and signal distortion during live broadcasting. The use of photonic MMW wireless linking in such applications involves connecting several HDTV cameras, each with a data rate of 1.5 Gbit s^{-1} , to a broadcast van via optical fiber. In the broadcast van, the multi-channel HDTV optical data are converted to an MMW signal centered at around 100 GHz and then radiated to a relay point using a photonic transmitter with a high-directivity antenna.

Another important commercial application of MMW wireless linkage for consumer electronics is in the 60 GHz band (e.g. SiBEAM). Applications include wireless linking for high-definition multimedia interface (HDMI) and high-speed data transfer between cell phones and digital cameras. However, to date, photonic technology has not been essential in order to realize 60 GHz indoor wireless linking. The major challenge for MMW photonic wireless linking is the cost of the technology and strong competition with the all-electronic approach [3]. As the CMOS IC technology matures, it is now possible to install MMW CMOS local-oscillator chips (Figure 1(b)) in each base station without requiring a synchronized local oscillator signal [3]. Furthermore, if the MMW output power from the base station is sufficiently strong, the links could be made directly with the base station without using optical fiber. However, MMW (>60 GHz) has optical behavior, such as straight-line propagation and subject to shading by obstacles in the transmission path. Numerous remote antenna units would therefore be needed at the user end to increase network coverage. This is a particularly important issue for outdoor wireless linking systems. Compared with the all-electronic approach, the most important advantage of the photonic technique is that the use of a fiber backbone to interconnect and synchronize the units minimizes the problems of interference and multi-path effects between these units, providing better immunity to bad weather conditions. Overall, lowering the cost of photonic MMW

technology will be one of the dominating factors in making the technology commercially viable for gigabit wireless linking. Recently, some of the key components and systems, which include photonic transmitters for 75–180 GHz [85], 60 GHz electro-absorption modulators, and compact 60 GHz photonic-wireless linking systems [86], have been commercialized (e.g. IPHOBAC, www.ist-iphobac.org) to meet the challenges of the coming wireless gigabit era. Figure 10 shows a photograph of a commercial UTC photodiode-based photonic transmitter from NTT (Japan). As can be seen, the delicate MMW waveguide output and optical input package of such a module allows easy integration with an MMW antenna or amplifier for RoF applications.

References

- M. Lazarus, *IEEE Spectrum* **47**, No. 10, 26 (2010).
- Y. Kado, M. Shinagawa, H.-J. Song, T. Nagatsuma, *Prog. Electromagnetics Res. Symp.* **2010**, 777 (2010).
- A. Hirata *et al.*, *J. Lightwave Technol.* **26**, 2338 (2008).
- M. Weiss *et al.*, *J. Lightwave Technol.* **26**, 2424 (2008).
- J. Wells, *IEEE Microwave Magazine* **18**, 104 (2009).
- H.-J. Song *et al.*, *IEEE Int. Topical Meeting Microwave Photon.* **2010**, 42 (2010).
- G. Ducournau *et al.*, *Electron. Lett.* **46**, 1349 (2010).
- J. Federici, L. Moeller, *J. Appl. Phys.* **107**, 111101 (2010).
- A.-M. Niknejad, H. Hashemi, *mm-Wave Silicon Technology: 60 GHz and Beyond* (Springer-Verlag, USA, 2008).
- J. Lee, Y. Huang, Y. Chen, H. Lu, C. Chang, *Int. Solid-State Circuits Conf.*, 316 (2009).
- H. Takahashi *et al.*, *IEEE MTT-S Int. Microwave Symp.* **2010**, 632 (2010).
- R. Yamaguchi *et al.*, *IEEE Radio and Wireless Symp.* **2008**, 695 (2008).
- J. Hacker *et al.*, *IEEE MTT-S Int. Microwave Symp.* **2010**, 1126 (2010).
- J.-D. Albrecht *et al.*, *IEEE MTT-S Int. Microwave Symp.* **2010**, 1118 (2010).
- M.-J. Crisp *et al.*, *IEEE LEOS Newsletter* **23**, 16 (2009).
- A.-J. Seeds, K.-J. Williams, *J. Lightwave Technol.* **24**, 4628 (2006).
- J. Capmany, D. Novak, *Nature Photonics* **1**, 319 (2007).
- M. Weiss *et al.*, *Int. Topical Meeting Microwave Photon.* **2009**, 1 (2009).
- J. Jiang *et al.*, *ECOC 2010*, Th.9.B.5 (2010).
- H.-J. Song *et al.*, *J. Lightwave Technol.* **26**, 2521 (2008).
- C.-T. Lin *et al.*, *IEEE Trans. Microwave Theory Tech.* **57**, 2084 (2009).
- F.-M. Kuo *et al.*, *IEEE Photonics J.* **2**, 719 (2010).
- T. Kawanishi *et al.*, *IEEE Photon. Technol. Lett.* **17**, 669 (2005).
- A. Hirata, H. Ishii & T. Nagatsuma, *IEEE Trans. Microwave Theory Tech.* **49**, 2157 (2001).
- Y.-S. Wu, N.-W. Chen & J.-W. Shi, *IEEE Photon. Technol. Lett.* **20**, 1799 (2008).
- H.-G. Bach *et al.*, *OFC/NFOEC 2008*, OMK1 (2008).
- S. M. Duffy *et al.*, *IEEE Trans. Microwave Theory Tech.* **49**, 1032 (2001).
- K. Kato, *IEEE Trans. Microwave Theory Tech.* **47**, 1265 (1999).
- D.-A. Tulchinsky *et al.*, *J. Lightwave Technol.* **26**, 408 (2008).
- A. Hirata, T. Kosugi, N. Meisl, T. Shibata, T. Nagatsuma, *IEEE Trans. Microwave Theory Tech.* **52**, 1843 (2004).
- H.-J. Tsai, N.-W. Chen, F.-M. Kuo, J.-W. Shi, *IEEE MTT-S Int. Microwave Symp.* **2010**, 740 (2010).
- N.-W. Chen, H.-J. Tsai, F.-M. Kuo, J.-W. Shi, *IEEE Trans. Microwave Theory Tech.* DOI: 10.1109/TMTT.2011.2104977 (2011).
- T. Ohno *et al.*, *Electron. Lett.* **39**, 520 (2003).
- T. Ohno, F. Nakajima, T. Furuta, H. Ito, *Electron. Lett.* **41**, 1057 (2005).
- S. Kawanishi, M. Saruwatari, *IEEE Trans. Instrumentation and Measurement* **38**, 569 (1989).
- Z.-F. Fan, N. Dagenais, *IEEE Trans. Microwave Theory Tech.* **45**, 1296 (1997).
- J. C. Pearson, P. Chen, H. M. Pickett, *SPIE* **4855**, 459 (2003).
- R. Hofstetter, H. Schmuck, R. Heidemann, *IEEE Trans. Microwave Theory and Tech.* **43**, 2263 (1995).
- C.-B. Huang, S.-G. Park, D. E. Leaird, A. M. Weiner, *Opt. Express* **16**, 2520 (2008).
- T. Sakamoto, T. Kawanishi, M. Izutsu, *Opt. Lett.* **32**, 1515 (2007).
- A. Hirata, M. Harada, T. Nagatsuma, *J. Lightwave Technol.* **21**, 2145 (2003).
- K. Okamoto, *Fundamentals of Optical Waveguides* (Academic Press, USA, 2005).
- P.-T. Shih *et al.*, *J. Lightwave Technol.* **28**, 71 (2010).
- C.-T. Lin *et al.*, *IEEE Photon. Technol. Lett.* **20**, 1027 (2008).
- Z. Jiang, C.-B. Huang, D. E. Leaird, A. M. Weiner, *Nature Photon.* **1**, 463 (2007).
- C.-B. Huang, D. E. Leaird, A. M. Weiner, *Opt. Lett.* **32**, 3242 (2007).
- C.-B. Huang, D. E. Leaird, A. M. Weiner, *IEEE Photon. Technol. Lett.* **21**, 1287 (2009).
- H.-P. Chuang & C.-B. Huang, *Opt. Express* **18**, 24003 (2010).
- H. Maestre, A. J. Torregrosa, C. R. Fernández-Pousa, J. A. Pereda, J. Capmany, *IEEE J. Quantum Electron.* **46**, 1681 (2010).

50. C.-S. Friedrich *et al.*, *IEEE J. Sel. Topics Quantum Electron.* **14**, 270 (2008).
51. M. Y. Jeon *et al.*, *Opt. Express* **18**, 12291 (2010).
52. C.-H. Yeh *et al.*, *IEEE Photon. Technol. Lett.* **21**, 125 (2009).
53. S.-C. Chan, R. Diaz, J.-M. Liu, *Opt. Quantum Electron.* **40**, 83 (2008).
54. L. A. Johansson, A. J. Seeds, *IEEE MTT-S Int. Microwave Symp.* **2000**, 1737 (2000).
55. Y.-S. Juan, Y.-C. Chen, F.-Y. Lin, *Proc. SPIE* **7936**, 793609 (2010).
56. J.-W. Shi, F.-M. Kuo, M.-Z. Chou, *OFC/NFOEC 2010*, PDP 6 (2010).
57. F.-M. Kuo, M.-Z. Chou, J.-W. Shi, *J. Lightwave Technol.* **29**, 432 (2011).
58. J.-W. Shi *et al.*, *IEEE J. Quantum Electron.* **46**, 80 (2010).
59. J.-W. Shi *et al.*, *IEEE Photon. Technol. Lett.* **17**, 1722 (2005).
60. M. R. Melloch, N. Otsuka, J. M. Woodall, A. C. Warren, J. L. Freeouf, *Appl. Phys Lett.* **57**, 1531 (1990).
61. S. Gupta, J. F. Whitaker, G. A. Mourou, *IEEE J. Quantum Electron.* **28**, 2464 (1992).
62. J.-W. Shi *et al.*, *IEEE Photon. Technol. Lett.* **13**, 623 (2001).
63. J.-W. Shi *et al.*, *IEEE Photon. Technol. Lett.* **14**, 1587 (2002).
64. S. Y. Chou, M. Y. Liu, *IEEE J. Quantum Electron.* **28**, 2358 (1992).
65. L. Möller *et al.*, *Opt. Lett.* **33**, 393 (2008).
66. T.-A. Liu, G.-R. Lin, Y.-C. Chang, C.-L. Pan, *Opt. Express* **13**, 10416 (2005).
67. Y.-T. Li *et al.*, *IEEE J. Quantum Electron.* **46**, 19 (2010).
68. S. Verghese, K. A. McIntosh, E. R. Brown, *IEEE Trans. Microwave Theory Tech.* **45**, 1301 (1997).
69. A. J. Lochtefeld, M. R. Melloch, J. C. P. Chang, E. S. Harmon, *Appl. Phys Lett.* **69**, 1465 (1996).
70. H. Ito *et al.*, *IEEE J. Sel. Topics in Quantum Electron.* **10**, 709 (2004).
71. N. Li *et al.*, *IEEE Photon. Technol. Lett.* **16**, 864 (2004).
72. J.-W. Shi, Y.-S. Wu, C.-Y. Wu, P.-H. Chiu, C.-C. Hong, *IEEE Photon. Technol. Lett.* **17**, 1929 (2005).
73. Y.-S. Wu, J.-W. Shi, P.-H. Chiu, *IEEE Photon. Technol. Lett.* **18**, 938 (2006).
74. Y.-S. Wu, J.-W. Shi, *IEEE Photon. Technol. Lett.* **20**, 1160 (2008).
75. F.-M. Kuo *et al.*, *IEEE Electron Device Lett.* **30**, 1167 (2009).
76. A. Ueda *et al.*, *IEEE Trans. Microwave Theory Tech.* **51**, 1455 (2003).
77. A. Stöhr *et al.*, *J. Lightwave Technol.* **21**, 3062 (2003).
78. F.-M. Kuo *et al.*, *OFC/NFOEC 2010*, OTThF7 (2010).
79. J.-W. Shi *et al.*, *IEEE Int. Topical Meeting Microwave Photon. 2010*, 46 (2010).
80. F.-M. Kuo *et al.*, *IEEE Photon. J.* **3**, 209 (2011).
81. A. Hirata, T. Furuta, H. Ito, T. Nagatsuma, *J. Lightwave Technol.* **24**, 1725 (2006).
82. R. W. Ridgway, D. W. Nippa, S. Yen, *IEEE Trans. Microwave Theory Tech.* **58**, 3117 (2010).
83. R. Sambaraju *et al.*, *IEEE Int. Topical Meeting Microwave Photon. 2010* DOI: 10.1109/MWP.2010.5664135 (2010).
84. T. Nagatsuma, H. Ito, T. Ishibashi, *Laser & Photon. Rev.* **3**, 123 (2009).
85. T. Nagatsuma *et al.*, *IEEE Photonic Society Meeting 2010*, 385 (2010).
86. A. Stöhr, *IEEE Int. Topical Meeting Microwave Photon. 2010*, 7 (2010).

Author profiles



Jin-Wei Shi

Jin-Wei Shi received his BS degree in electrical engineering from National Taiwan University in 1998 and his PhD from the Graduate Institute of Electro-Optical Engineering from the same institution in 2002. He was a visiting scholar at the University of California, Santa Barbara, USA, from 2000 to 2001. In 2002–2003, he served as a postdoctoral researcher at the Electronic Research & Service Organization of the Industrial Technology Research Institute in Taiwan. He joined the Department of Electrical Engineering at National Central University, Taoyuan, Taiwan, in 2003 where he is now associate professor. His current research interests include ultrahigh-speed/power optoelectronic devices, such as photodetectors, electro-absorption modulators, sub-millimeter-wave photonic transmitters and semiconductor lasers.



Chen-Bin Huang

Chen-Bin Huang received his BS degree in electrical engineering from National Tsing Hua University in Taiwan in 1997, his MS degree in electro-optical engineering from National Chiao Tung University, Taiwan, in 1999, and his PhD degree from the School of Electrical and Computer Engineering at Purdue University, Indiana, USA, in 2008. He has worked at Bell Laboratories (Alcatel-Lucent) in the USA, the Opto-Electronics & Systems Laboratories of the Industrial Technology Research Institute in Taiwan, and the Materials Research Institute at Northwestern University, Illinois, USA. He joined the Institute of Photonics Technologies at National Tsing Hua University as assistant professor in 2008. His current research interests include optical and radiofrequency arbitrary waveform generations, applications of optical frequency combs and nanophotonics.



Ci-Ling Pan

Ci-Ling Pan received his PhD degree in physics from Colorado State University in the USA in 1979. He is currently Tsing Hua Chair Professor of the Department of Physics and Institute of Photonics Technologies, and director of the Photonics Research Center of National Tsing Hua University in Taiwan. Prior to 2009, he was University Chair Professor and founding chair of the Department of Photonics and director of the Institute of Electro-Optical Engineering at National Chiao Tung University in Taiwan. His research interests include ultrafast and tunable lasers, ultrafast optoelectronics, THz science and technology, optical and millimeter-wave interactions, and fiber and liquid-crystal optics.